Energy Engineering

Tech Science Press

Doi:10.32604/ee.2025.073042

ARTICLE

Boundary Decision-Based Multi-Objective Robust Optimization for Microgrid Dispatching

Junjian Wu, Jingliao Sun*, Yejun Xiang, Zhenyu Zhou and Zhengchai Shi

Electric Power Dispatching and Control Center, State Grid Wenzhou Electric Power Supply Company, Wenzhou, 325000, China

*Corresponding Author: Jingliao Sun. Email: sunjingliao@163.com

Received: 09 September 2025; Accepted: 03 December 2025; Published: 18 June 2026

ABSTRACT: The inherent unpredictability of renewable energy generation poses significant challenges to the reliable and economic dispatch of grid-connected microgrids. In response, this paper proposes a novel robust optimization strategy grounded in uncertain boundary decision-making and enhanced through innovations in the multi-objective cross-entropy method. An uncertainty budget-aware environmental economic dispatch model is first established, integrating photovoltaic and wind power generation. By employing mathematical sophistication—particularly Lagrangian transformation—the proposed method effectively resolves embedded uncertainties, transforming the original model into a deterministic multi-objective optimization framework robust against renewable energy volatility. Furthermore, by incorporating the dynamic operational demands of microgrids, this paper culminates in a robust optimization approach that is both fundamentally based on and adaptively responsive to uncertainty boundaries. To address the critical challenges of convergence and diversity in multi-objective optimization, crossover operators and an adaptive parameter update mechanism are introduced, significantly refining the conventional multi-objective cross-entropy algorithm. Case studies demonstrate the rationality and effectiveness of the proposed dispatch strategy and corroborate the superior performance and applicability of the enhanced algorithm.

KEYWORDS: Microgrid; environmental economic dispatch; uncertain boundary; robust optimization; multi-objective cross entropy algorithm

1 Introduction

Microgrid (MG) has garnered significant research interest due to its flexible and efficient energy management capabilities. By integrating Renewable Energy Generation (REG), energy storage systems, and intelligent control technologies [1], microgrids have optimized the allocation and utilization of power resources, offering efficient and clean dispatch solutions. However, the inherent uncertainties associated with REG, such as output fluctuations and randomness, pose significant challenges to the secure and economic dispatch of microgrids [2,3]. Addressing these uncertainties to ensure stable system operation has become a critical research focus.

Traditional optimization methods for dispatch primarily rely on deterministic analyses, which often fail to adequately account for the impact of uncertainties on dispatch outcomes. To handle the uncertainties in microgrid systems, various uncertainty-based optimization methods have been developed. Among these, the mainstream approaches include Stochastic Optimization (SO) [4,5], Chance Constrained Programming (CCP) [6,7], and Robust Optimization (RO) [8,9]. Stochastic Optimization (SO) relies on known and accurate probability distributions of uncertainties, simplifying problems into deterministic scenarios. However,

Copyright © 2026 The Authors. Published by Tech Science Press.
This work is licensed under a Creative Commons Attribution 4.0 International License, which permits unrestricted use, distribution, and reproduction in any medium, provided the original work is properly cited.

accurately capturing uncertainties often requires numerous scenarios, which is impractical. RO, noted for its independence from probability distributions, ensures dispatch solution feasibility even in adverse conditions by using uncertainty sets to define renewable energy generation fluctuations [10,11]. This set-based approach eliminates the need for precise probabilistic knowledge and constructs robust objective function models under extreme scenarios. Literature [12] introduces a robust multi-objective optimization dispatch method for microgrids, employing robust measures to describe uncertain factors. Literature [13] proposes a planning method for distributed energy storage systems in microgrids under emergency reserve constraints, analyzing the worst-case scenarios of photovoltaic output volatility through robust optimization. Typically, RO can be categorized based on the characteristics of the uncertainty sets into box-based robust optimization [14] and ellipsoidal-based robust optimization [15]. Box-based robust optimization defines uncertainty sets through linear constraints, enabling efficient solutions for linear mathematical models [16,17]. However, its strategy of sacrificing economic efficiency for robustness often results in conservative outcomes. To strike a balance, D. Bertsimas et al. introduced the concept of "price of robustness," allowing for flexible adjustments between economic efficiency and robustness by varying the price of robustness [18]. This approach provides an effective solution for practical needs, enabling more flexible decision-making in the face of uncertainties. Accordingly, to address the uncertainties in renewable energy output, this paper establishes a robust optimization model for the environmental and economic dispatch of microgrids. Through mathematical theories such as Lagrangian transformation, the model eliminates uncertain variables, deriving an improved robust optimization method with uncertain boundary decisions, offering a balanced solution for practical dispatch scenarios. Furthermore, for the deterministic environmental and economic dispatch model post-decision, the need to balance economic efficiency and environmental protection in the optimal solution necessitates the use of efficient and adaptable multi-objective optimization algorithms to solve the problem.

The Cross-Entropy Algorithm (CE), a trailblazing metaheuristic, orchestrates the refinement of elite samples and the genesis of new populations by resampling rare events and minimizing the Kullback-Leibler divergence. Renowned for its adaptable algorithmic architecture and streamlined population update mechanism, CE has carved a niche in solving diverse engineering conundrums [19]. However, the algorithm's limitations are also notable: a tendency to converge to local optima and a reliance on predefined smoothing parameters. Multi-objective optimization algorithms spawned from CE often inherit these inherent flaws [20,21]. To circumvent these pitfalls, adaptive update operators are introduced to supplant the preset parameter process, and crossover operators are integrated to eschew local optima entrapment. By amalgamating the non-dominated sorting mechanism of the NSGA-II (Nondominated Sorting Genetic Algorithm II), the EMOCE (External Files-Based Multi-Objective Cross-Entropy Algorithm) is unveiled. Conclusively, leveraging the proposed boundary decision-adjustable robust optimization strategy, the EMOCE algorithm is deployed to scrutinize a case study involving the environmental and economic dispatch of renewable energy units, thereby substantiating the cogency of the decision-making paradigm and the efficacy and preeminence of the multi-objective algorithm.

2 Robust Optimization Method Based on Boundary Decision Strategy

2.1 Microgrid Optimization Model

2.1.1 Oriented Dispatch Model for Uncertain Renewable Energy Power Outputs

In modeling the fluctuations of Renewable Energy Generation, given its inherent variability, this study employs an interval to define the uncertain output ranges for Photovoltaic (PV) units and Wind Turbine (WT) units.

$$\begin{cases} \tilde{P}_{\mathrm{Re}i,t} = P_{\mathrm{Re}i,t} + \Delta P_{\mathrm{Re}i,t} \\ -\hat{P}_{\mathrm{Re}i,t} \leqslant \Delta P_{\mathrm{Re}i,t} \leqslant \hat{P}_{\mathrm{Re}i,t} \end{cases} \quad i \in N_{\mathrm{Re}} \tag{1}$$

In the equation, the notation $\tilde{P}_{\mathrm{Re}i,t}$ represents the actual output power of the renewable energy generation unit i at time period t, correspondingly, $P_{\mathrm{Re}i,t}$ denotes its forecasted output, and $\Delta P_{\mathrm{Re}i,t}$ measures the output fluctuation of the renewable energy generation station. The terms $\hat{P}_{\mathrm{Re}i,t}$ and $-\hat{P}_{\mathrm{Re}i,t}$ respectively signify the upper and lower bounds of the output fluctuation for unit i at time period t.

To analyze the volatility of this renewable energy during actual operation, the output fluctuation coefficient $\delta_{i,t}$ is introduced here, satisfying the following:

$$\delta_{i,t} = \frac{\Delta P_{\mathrm{Re}i,t}}{\hat{P}_{\mathrm{Re}i,t}} \tag{2}$$

$\delta_{i,t} \in [-1, 1]$ is used to quantify the fluctuation degree of the output of REG unit i at time period t in actual production. Based on this, the actual output of the REG unit can be expressed as:

$$\tilde{P}_{\mathrm{Re}i,t} = P_{\mathrm{Re}i,t} + \delta_{i,t}\hat{P}_{\mathrm{Re}i,t} \tag{3}$$

Introducing the concept of "Uncertainty Budget" to define the uncertainty of REG output:

$$\Gamma_t = \sum_{i \in N_{\mathrm{Re}}} |\delta_{i,t}| \tag{4}$$

Within the scope of this study, the uncertainty budget is defined as the absolute sum of the ratio between the actual output fluctuation of the REG units and their maximum fluctuation limit. This definition reveals the quantitative essence of system robustness. As the output fluctuation of REG increases, the model exhibits a stronger conservative tendency. This paper employs the concept of cost in economics to metaphorically describe this degree of conservatism, termed as uncertainty budget. The value of Γ_t serves as a quantitative indicator of this cost, where its increase or decrease directly reflects the robustness or aggressiveness of the model strategy: a larger Γ_t indicates a more conservative model, while a smaller Γ_t signifies a higher degree of model aggressiveness. In subsequent analyses, Γ_t will play a pivotal role in balancing the trade-off between model robustness and economic low-carbon objectives.

2.1.2 CAES Energy Storage Scheduling Model

In the section dedicated to the selection of energy storage systems, Compressed-Air Energy Storage (CAES) is chosen for its ease of deployment, environmental friendliness, and high overall efficiency [22,23].

$$\dot{p}_{\mathrm{G},t} = k_{\mathrm{G}} P_{\mathrm{G},t} \tag{5}$$

In the aforementioned equation, $\dot{p}_{\mathrm{G},t}$ denotes the rate of change of air pressure in the storage chamber during the power generation phases of the Compressed-Air Energy Storage system at time period t. $P_{\mathrm{G},t}$ represents the generation power of the CAES at time period t.

The simplified mathematical expression is:

$$p_{\mathrm{CAES},t} = p_{\mathrm{CAES},t-1} + u_{\mathrm{C},t} k_{\mathrm{C}} P_{\mathrm{C},t} \Delta t - u_{\mathrm{G},t} k_{\mathrm{G}} P_{\mathrm{G},t} \Delta t \tag{6}$$

$p_{\mathrm{CAES},t}$ represents the air pressure of the CAES at time interval t. The variables $u_{\mathrm{C},t}$ and $u_{\mathrm{G},t}$ correspond to the gas compression and expansion power generation scenarios at time interval t, respectively. The term Δt denotes the duration of the unit scheduling interval in day-ahead scheduling.

2.1.3 Diesel Generator Model

The diesel generator operates in two modes: constant power output and load-following operation. In the latter mode, as fuel consumption increases, the output power correspondingly rises. Considering the emission of polluting gases during the operation of the diesel generator [24], the cost components of the diesel generator are as follows:

$$\begin{cases} C_{DO,t} = K_{DO} P_{DE,t} \\ C_{DF,t} = \alpha P_{DE,t}^2 + \beta P_{DE,t} + \gamma \\ C_{DE,t} = \sum_{k=1}^{n} (C_k \gamma_{de,k}) P_{DE,t} \end{cases} \tag{7}$$

In the equation, $C_{DO,t}$ represents the operation and maintenance cost of the diesel generator at time interval t, $C_{DF,t}$ denotes the fuel cost, and $C_{DE,t}$ corresponds to the treatment cost of polluting gas emissions. $P_{DE,t}$ signifies the power generation at time interval t.

2.2 Robust Optimization Based on Boundary Decision-Making

2.2.1 Robust Optimization Day-Ahead Scheduling Model

This study employs a multi-objective framework to account for the non-negligible emissions produced by conventional generators. The emission treatment cost is adopted as a well-established, proportional proxy for the environmental objective, offering a quantifiable measure despite encapsulating only one facet of the broader ecological impact.

REG, CAES, and diesel generation participate in power scheduling, where the output of REG is robustly treated due to its uncertain nature. The system aims to minimize the economic cost of operation and the cost of emission treatment, with the objective function being:

$$\begin{cases} \min F_1 = C_{REG} + C_{CAES} + C_{DE} \\ \min F_2 = C_{EMI} = \sum_{t=1}^{T} \sum_{k=1}^{n} (C_k \gamma_{de,k}) P_{DE,t} \\ C_{\mathrm{CAES}} = \sum_{t=1}^{T} c_{\mathrm{G}} P_{\mathrm{G},t} \\ C_{\mathrm{REG}} = \sum_{t=1}^{T} \sum_{i \in N_{\mathrm{REG}}} c_{\mathrm{REG}} \delta_{i,t} \hat{P}_{\mathrm{REG}i,t} \end{cases} \tag{8}$$

In the above formula, C_{CAES} represents the economic cost of expansion generation of the CAES unit within the scheduling period; C_{DE} represents the operating economic cost of the diesel generator set; C_{REG} is introduced as an economic penalty cost for the uncertainty of REG output; C_{EMI} represents the emission treatment cost of the diesel generator.

The current constraints in day-ahead scheduling primarily include the following:

$$\tilde{P}_{REG,t} + u_{G,t} P_{G,t} + P_{DE,t} = P_{AL,t} + u_{C,t} P_{C,t} \tag{9}$$

$$P_{\mathrm{REG}i,min} \leqslant \tilde{P}_{\mathrm{REG}i,t} \leqslant P_{\mathrm{REG}i,max} \tag{10}$$

$$P_{\mathrm{DG,min}} \leqslant P_{\mathrm{DG},t} \leqslant P_{\mathrm{DG,max}} \tag{11}$$

$$P_{\mathrm{G,min}} \leqslant P_{\mathrm{G},t} \leqslant P_{\mathrm{G,max}} \tag{12}$$

$$p_{\mathrm{gsc,min}} \leqslant p_{\mathrm{gsc},t} \leqslant p_{\mathrm{gsc,max}} \tag{13}$$

$$\tilde{P}_{\mathrm{REG},t} + u_{\mathrm{G},t}P_{\mathrm{G,max}} + P_{\mathrm{DG,max}} \geqslant P_{\mathrm{AL},t}(1+L\%) \tag{14}$$

$P_{AL,t}$ represents the total load power during time period t. $P_{\mathrm{DG,max}}$ and $P_{\mathrm{DG,min}}$ represent the upper and lower limits of diesel generator output, respectively. $P_{\mathrm{G,max}}$ and $P_{\mathrm{G,min}}$ represent the upper and lower limits of the CAES expansion power generation output, respectively.

2.2.2 Transformation of Uncertain Variables in Constraints

In the scheduling model discussed previously, the presence of the uncertain variable $\tilde{P}_{\mathrm{REG},t}$ in the spinning reserve constraint, specifically in Formula (14), complicates the solution process. The following section employs mathematical techniques to transform this uncertain variable, thereby facilitating the resolution of the constraint.

Initially, substituting Eqs. (1) and (12) into Eq. (14) yields:

$$\sum_{i\in N_{\mathrm{REG}}} \Delta P_{\mathrm{REG}i,t} \leqslant \left[\left(P_{\mathrm{DG,max}} + u_{\mathrm{G},t}P_{\mathrm{G,max}}\right) - (1+L\%)\cdot\left(P_{\mathrm{DG},t} + u_{\mathrm{G},t}P_{\mathrm{G},t} - u_{\mathrm{C},t}P_{\mathrm{C},t}\right)\right]/L\% - \sum_{i\in N_{\mathrm{REG}}} P_{\mathrm{REG}i,t} \tag{15}$$

Formula (15) can be equivalently transformed into:

$$max \sum_{i\in N_{\mathrm{REG}}} \Delta P_{\mathrm{REG}i,t} \leqslant \left[\left(P_{\mathrm{DG,max}} + u_{\mathrm{G},t}P_{\mathrm{G,max}}\right) - (1+L\%)\cdot\left(P_{\mathrm{DG},t} + u_{\mathrm{G},t}P_{\mathrm{G},t} - u_{\mathrm{C},t}P_{\mathrm{C},t}\right)\right]/L\% - \sum_{i\in N_{\mathrm{REG}}} P_{\mathrm{REG}i,t} \tag{16}$$

Then, based on linear duality theory, the maximum value problem can be symmetrically transformed into a minimum value problem:

$$max \sum_{i\in N_{\mathrm{REG}}} \Delta P_{\mathrm{REG}i,t} = -min\left(-\sum_{i\in N_{\mathrm{REG}}} \Delta P_{\mathrm{REG}i,t}\right) \tag{17}$$

Construct the Lagrangian function of $-min\left(-\sum_{i\in N_{\mathrm{REG}}} \Delta P_{\mathrm{REG}i,t}\right)$ to obtain:

$$\begin{aligned} L = &-\sum\nolimits_{i\in N_{\mathrm{REG}}} \Delta P_{\mathrm{REG}i,t} + \mu_t \sum\nolimits_{i\in N_{\mathrm{REG}}} \Delta P_{\mathrm{REG}i,t} + \lambda_{1t}\left[\sum\nolimits_{i\in N_{\mathrm{REG}}} \Delta P_{\mathrm{REG}i,t} - \left(\sum\nolimits_{i\in N_{\mathrm{REG}}} -\hat{P}_{\mathrm{REG}i,t}\right)\right] \\ &+ \lambda_{2t}\left(\sum\nolimits_{i\in N_{\mathrm{REG}}} \hat{P}_{\mathrm{REG}i,t} - \sum\nolimits_{i\in N_{\mathrm{REG}}} \Delta P_{\mathrm{REG}i,t}\right) \end{aligned} \tag{18}$$

Using the KKT conditions, the following can be obtained:

$$\begin{cases} -1 + \mu_t + \lambda_{1t} - \lambda_{2t} = 0 \\ \lambda_{1t} \geqslant 0, \lambda_{2t} \geqslant 0 \end{cases} \tag{19}$$

Finally, by combining Formulas (15) to (19) and collecting like terms, the spinning reserve constraint in Formula (14) is transformed into:

$$\begin{cases} P_{\mathrm{DG},t} + u_{\mathrm{G},t}P_{\mathrm{G},t} - u_{\mathrm{C},t}P_{\mathrm{C},t}\left\{P_{\mathrm{DG,max}} + u_{\mathrm{G},t}P_{\mathrm{G,max}} - \right. \\ L\%[\sum\limits_{i\in N_{\mathrm{REG}}} P_{\mathrm{REG}i,t} + (\lambda_{1,t} + \lambda_{2,t}) \sum\limits_{i\in N_{\mathrm{REG}}} \delta_{i,t}\hat{P}_{\mathrm{REG}i,t}]] \\ /(1 + L\%) \\ \lambda_{1,t}0, \lambda_{2,t}0 \end{cases} \tag{20}$$

The practical significance of this transformation lies in the fact that the upper limit of power output fluctuations for renewable energy sources, such as photovoltaic units, denoted as $\hat{P}_{\mathrm{REG}i,t}$, is typically given before scheduling. Therefore, the transformation effectively eliminates the uncertain variable. Additionally, the degree of fluctuation for REG, represented by $\delta_{i,t}$, can be selected based on the actual needs of the site.

2.2.3 Robust Optimization with Proactive Boundary Decision Method

In the context of microgrid scheduling, the fluctuation of REG directly affects the probability of violating system reserve constraints, while the uncertainty robustness cost Γ_t quantifies the overall fluctuation degree of REG. Boundary decision-making refers to the scheduling plan made when the power output of units reaches the boundary of constraints under extreme scenarios. Consider a scenario where, during time period t, the absolute values of the power fluctuation coefficients of $N-1$ renewable energy units are equal to 1, forming a set S; only one REG unit has a power fluctuation coefficient with an absolute value less than 1, denoted as M. According to the derivation process in literature [25], the probability of violating the spinning reserve constraint in this scenario satisfies:

$$P_{\mathrm{r}}\left(\sum_{i=1}^{N_{\mathrm{REG}}} \tilde{P}_{\mathrm{REG}i,t} + u_{\mathrm{G},t}P_{\mathrm{G},t} + P_{\mathrm{DG,max}} < P_{\mathrm{AL},t}(1 + L\%) + u_{\mathrm{C},t}P_{\mathrm{C},t}\right) \leqslant P_{\mathrm{r}}\left(\sum_{i=1}^{N_{\mathrm{REG}}} \gamma_{i,t}\delta_{i,t} \geqslant \Gamma_t\right) \tag{21}$$

By applying the law of total probability to Formula (21) yields:

$$P_{\mathrm{r}}\left(\sum_{i=1}^{N_{\mathrm{REG}}} \gamma_{i,t}\delta_{i,t} \geqslant \Gamma_t\right) \leqslant \exp\left(-\frac{\Gamma_t^2}{2N_{\mathrm{REG}}}\right) \tag{22}$$

By integrating Formulas (21) and (22), the following result is obtained:

$$P_{\mathrm{r}}\left(\sum_{i=1}^{N_{\mathrm{REG}}} \tilde{P}_{\mathrm{REG}i,t} + u_{\mathrm{G},t}P_{\mathrm{G},t} + P_{\mathrm{DG,max}} < P_{\mathrm{AL},t}(1 + L\%) + u_{\mathrm{C},t}P_{\mathrm{C},t}\right) \leqslant \exp\left(-\frac{\Gamma_t^2}{2N_{\mathrm{REG}}}\right. \tag{23}$$

If the constraint is required to be satisfied with a probability of at least $1-\sigma$, then at least the following must be met:

$$\Gamma_t \geq \sqrt{-2N_{\mathrm{REG}}\ln(\sigma)} \tag{24}$$

where σ represents the probability of violating the reserve constraint.

Define the ratio of the robustness cost Γ_t to the number of REG units N_{REG} as the robustness cost coefficient, denoted by k, and let ξ represent the probability of constraint violation. According to Formulas (22) and (23), an increase in the number of connected REG units reduces the probability of spinning reserve capacity violation, thereby enhancing system stability.

In this study, taking the case of $N_{\mathrm{REG}} = 2$, the relationship between k and ξ is illustrated in Fig. 1. As shown in Fig. 1, a decrease in the robustness cost coefficient leads to an increase in the violation probability, indicating a weakened ability of the system to cope with the uncertainty of the REG output. Therefore, it is necessary to properly set and adjust the uncertainty budget to optimize system scheduling.

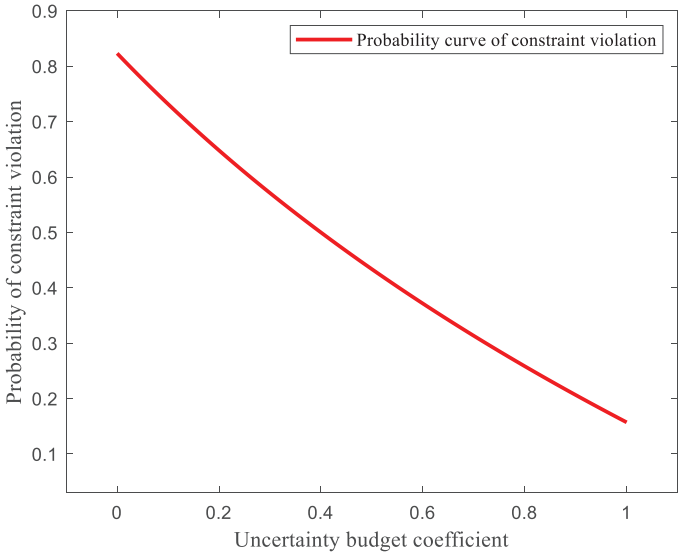

Figure 1: Relationship of robustness cost coefficient and constraint violation probability when $N_{\mathrm{REG}} = 2$

When the uncertainty budget Γ_t equals the total number of REG units N_{REG}, the constraint confidence level attains its maximum value ψ, signifying the system's peak resilience to uncertainties. In essence, $\Gamma_t = N_{\mathrm{REG}}$ achieves the confidence apex ψ. Formula (25) reveals that increasing the number of REG units N_{REG} elevates the maximum attainable confidence apex ψ, thereby enhancing systemic resilience.

$$\psi = 1 - \frac{1}{2^{N_{\mathrm{REG}}}} \tag{25}$$

Building upon the foregoing, the core execution process of the boundary-decision-based robust optimization can be summarized in Fig. 2.

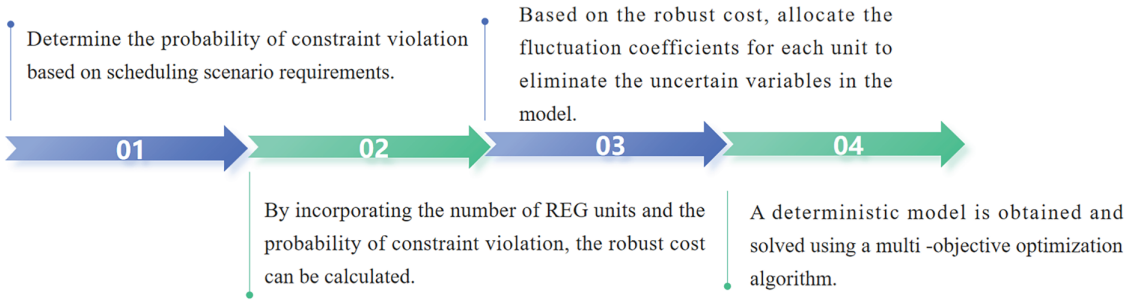

Figure 2: Multi objective robust optimization based on boundary decision-making

The proposed uncertainty boundary framework enables scenario-adaptive selection of Γ_t, achieving a Pareto-optimal equilibrium between robustness guarantees and economic/low-carbon objectives.

2.3 Improved Multi-Objective Cross-Entropy Method

2.3.1 Cross-Entropy Method

The Cross-Entropy Method (CE), first proposed by Rubinstein (1997), was originally designed for importance sampling and Kullback-Leibler divergence computation, later generalized to continuous and combinatorial optimization.

The CE algorithm is briefly summarized as follows: The algorithm initializes a population of N_p solutions with dimensionality D, where each dimension n is bounded within $[l_n, u_n]$. Parameters are initialized with mean μ_n and variance $\sigma_n^2(\sigma_n = 10 \cdot (u_n - l_n))$. During the k-th iteration, the i-th candidate solution is represented as:

$$X_i^k = \left(x_1^k, x_2^k, \ldots, x_D^k\right) \tag{26}$$

wherein, for each dimension, the value is taken as:

$$x_n^k = \mu_n + \text{randn}() * \sigma_n^2 \tag{27}$$

Subsequently, the algorithm selects an elite subset X_{elite} (size: $\rho \cdot N_p, \rho \in [0.1, 0.2]$) by ranking solutions based on fitness values. This subset drives iterative updates of the mean μ_n and variance σ_n^2.

$$X_{elite,n}(k) = \left(x_n^1, x_n^2, \ldots, x_n^{\rho \times N_p} \right) \tag{28}$$

$$\mu(k+1) = \alpha\mu(k+1) + (1-\alpha)\mu(k) \tag{29}$$

$$\sigma(k+1) = \beta\sigma(k+1) + (1-\beta)\sigma(k) \tag{30}$$

In the optimization process, the CE algorithm iteratively updates the mean and standard deviation using smoothing parameters α and β (typically within $[0.7, 1]$). The updated statistics are then employed to generate new population samples. The algorithm performs global search iterations, reconstructs the population, and selects elite individuals based on fitness rankings. This cycle repeats until the maximum iteration limit is reached, concluding the optimization.

2.3.2 Improved Multi-Objective Cross-Entropy Method

The core enhancements of EMOCE include three key aspects:

(1) Fast non-dominated sorting for elite solution selection, coupled with an external archive to preserve Pareto front diversity;

(2) A crossover operator to expand the search space and enhance solution diversity, thereby overcoming local optima entrapment and improving scalability for medium-large problems;

(3) An adaptive parameter update mechanism that dynamically adjusts the mean and standard deviation through self-learning, eliminating the need for preset constants while ensuring convergence.

The flowchart of the EMOCE algorithm is shown in Fig. 3.

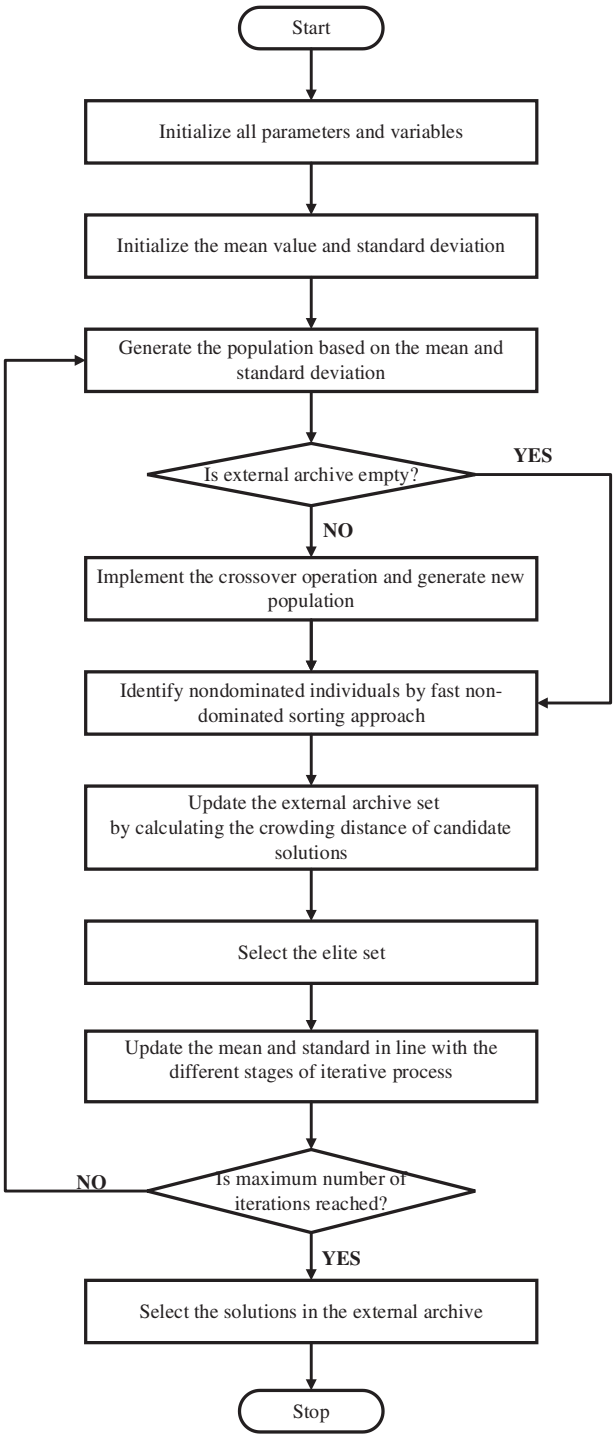

Figure 3: Flowchart of EMOCE algorithm

The mechanisms of these enhancements are briefly introduced as follows:

(1) Crossover operator

The EMOCE algorithm integrates a crossover strategy to enhance solution diversity and expand search space within feasible regions. Specifically: (1) Randomly select an individual X_i from the current population

and an elite solution X_j from the archive. (2) Perform partial parameter exchange between the paired solutions under a predefined crossover probability, generating two new offspring through recombination:

$$x_i^{new} = \begin{cases} x_j^n, rand < P_c \\ x_i^n, else \end{cases}, x_j^{new} = \begin{cases} x_i^n, rand < P_c \\ x_j^n, else \end{cases} \tag{31}$$

Herein, x_i^{new} and x_j^{new} denote the newly generated individuals after crossover, while $P_c \in [0,1]$ represents the crossover probability.

(2) The establishment and update of the external archive set

The crossover operator serves as the core mechanism for expanding the search domain and circumventing local optima, relying on the information exchange between newly generated solutions and those stored in the external archive named A_r. As a repository for non-dominated solutions, the external archive is updated iteratively using the fast non-dominated sorting mechanism from the NSGA-II algorithm.

(3) Diversification & enhancement stage

To enhance solution diversity and accelerate convergence, this study draws on the concept from Reference [26] and divides the iterative process into two phases: diversification and intensification, each with distinct strategies for updating the mean and standard deviation. As the names suggest, the diversification phase emphasizes expanding the distribution diversity of multi-objective solutions, while the intensification phase focuses on deep exploitation. Consequently, the selection of this transition point becomes particularly crucial. To address this, a series of experiments were conducted to systematically investigate the optimal transition point selection. Fig. 4 illustrates the performance of both the convergence metric (Convergence) and diversity metric (Spacing) for ZDT1 as the transition point varies from 40% to 80% of the maximum function evaluations. The results indicate that the Spacing metric achieves its optimum within the 50%–60% range, while the Convergence metric reaches its best value precisely at the 60% transition point. Considering the need to balance solution convergence and distribution, the transition point is consequently set at 60% of the maximum iterations. The results for transition points below 40% and above 80% are omitted due to their significantly larger metric values.

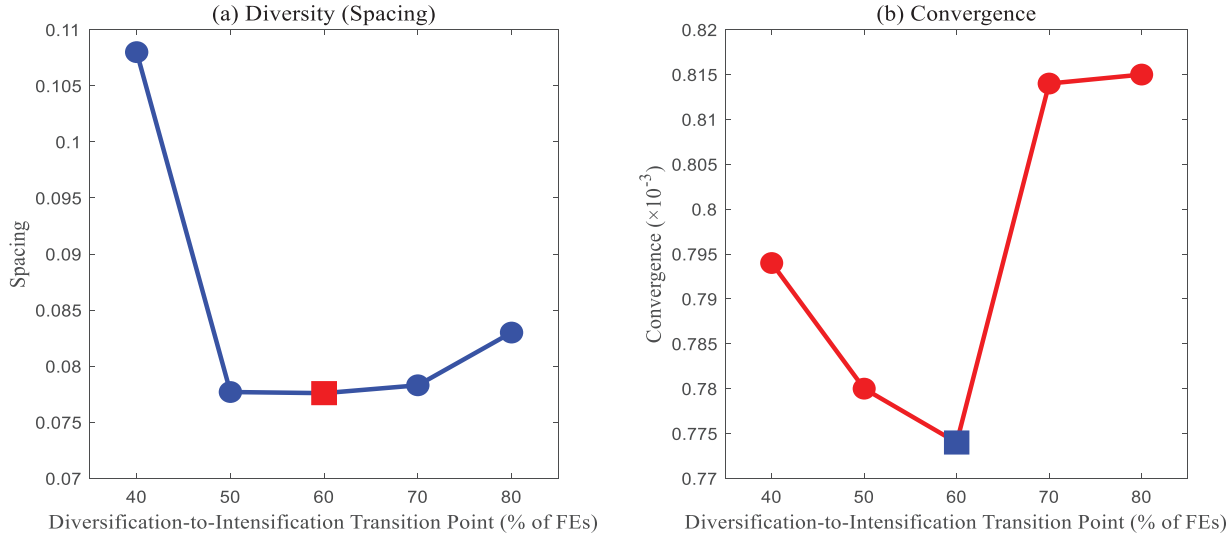

Figure 4: Convergence and diversity metrics of EMOCE under varied phase transition points

Furthermore, Tables 1 and 2 provides computed Spacing and Convergence values for ZDT1 and UF test suites under varying transition points, offering additional validation for the rationale behind selecting 60% of the maximum evaluations as the diversification-to-intensification switch in the EMOCE algorithm.

The bolded data in the table indicate that they are the minimum value in their respective row and therefore represent the optimal value. When the transition point is set at 60% of the maximum evaluations, the Spacing value is superior in three out of the five test functions, and the Convergence value leads in almost all cases.

Table 1: EMOCE spacing values at different transition points

Test function	Transition point					
	40%	**50%**	**60%**	**70%**	**80%**	**90%**
ZDT1	0.1080	0.0777	**0.0776**	0.0783	0.0832	0.1203
ZDT2	0.0956	0.1761	**0.0823**	0.0856	0.0867	0.0855
ZDT3	0.8622	**0.4477**	0.4852	0.5633	0.8681	0.8222
UF1	1.0624	**0.9925**	0.9933	1.1408	1.6632	1.8308
UF3	0.9936	0.9595	**0.9036**	0.9842	1.2039	1.8595

Table 2: EMOCE convergence values at different transition points

Test function	Transition point					
	40%	**50%**	**60%**	**70%**	**80%**	**90%**
ZDT1	7.79E−04	7.78E−04	**7.74E−04**	8.14E−04	8.15E−04	9.04E−04
ZDT2	8.23E−04	7.43E−04	**7.22E−04**	7.90E−04	8.33E−04	9.22E−04
ZDT3	8.07E−04	6.88E−04	**6.57E−04**	6.96E−04	8.29E−04	9.07E−04
UF1	0.0066	**0.0048**	0.0052	0.0052	0.0058	0.0066
UF3	0.8230	0.4590	**0.4210**	0.4450	0.5212	0.4926

This empirically determined threshold ensures adequate exploration of the search space in the early stages while focusing on convergence refinement in the latter stages. Eqs. (32) and (33) represent the diversification phase, whereas Eqs. (34) and (35) correspond to the intensification phase.

$$\mu(k+1) = mean(elite(k)) \tag{32}$$

$$\sigma(k+1) = std\left(X^{\rho N_p}(k)\right) \tag{33}$$

$$\mu(k+1) = mean(A_r(k)) \tag{34}$$

$$\sigma(k+1) = std\left(X^{\rho N_p}(k)\right) \tag{35}$$

3 Results and Discussion

3.1 Function Test of the EMOCE Algorithm

To rigorously evaluate the optimization performance of the EMOCE algorithm, a comparative study was conducted against five classical multi-objective algorithms: NSGA-II, MOPSO, PAES-II, MODE, and MOEA/D. The performance assessment was carried out using two established multi-objective performance metrics: Generational Distance (GD) and Convergence. The benchmark test suites, including the DEB, ZDT, and UF series of standard test functions, were employed in the evaluation. Each algorithm was independently executed 30 times for every test function, with the maximum number of function evaluations (FEs) set to 15,000.

Similarly to Tables 1 and 2, the bolded data in Tables 3 and 4 also represent the optimal values within their respective rows. As summarized in Tables 3 and 4, EMOCE demonstrates superior performance in both Convergence and Generational Distance (GD) across the ZDT1-3 and UF1-2 test functions, outperforming all peer algorithms. This evidences its exceptional optimization convergence. Furthermore, the Pareto fronts obtained by EMOCE, visualized in Figs. 5 and 6 against the true benchmark, intuitively showcase its leading performance in both convergence and diversity.

Table 3: Convergence metric values of the algorithms

Test function	MODE	MOEA/D	MOPSO	NSGAII	PESAII	EMOCE
DEB	8.77E−04	0.0024	8.69E−04	8.66E−04	8.91E−04	**8.09E−04**
ZDT1	0.1671	0.1560	0.0528	0.6386	0.1074	**7.74E−04**
ZDT2	0.3508	1.1110	1.4718	0.7810	0.1433	**7.22E−04**
ZDT3	0.1170	0.2075	0.1208	0.4479	0.0593	**6.57E−04**
UF1	0.0430	0.3521	0.6460	0.4971	0.1573	**0.0052**
UF3	0.4351	0.4569	0.8361	0.5820	0.5811	**0.4210**

Table 4: Generational distance values of the algorithms

Test function	MODE	MOEA/D	MOPSO	NSGAII	PESAII	EMOCE
DEB	1.72E−04	4.79E−04	**1.59E−04**	1.73E−04	1.63E−04	1.78E−04
ZDT1	0.0176	0.0157	0.0057	0.0661	0.0112	**2.64E−04**
ZDT2	0.0354	0.1136	0.1746	0.2412	0.0149	**7.55E−04**
ZDT3	0.0214	0.0272	0.0215	0.0679	0.0107	**1.63E−04**
UF1	0.0078	0.0372	0.1380	0.0537	0.0171	**0.0012**
UF3	0.0068	0.0064	0.0563	0.0206	0.0139	**0.0045**

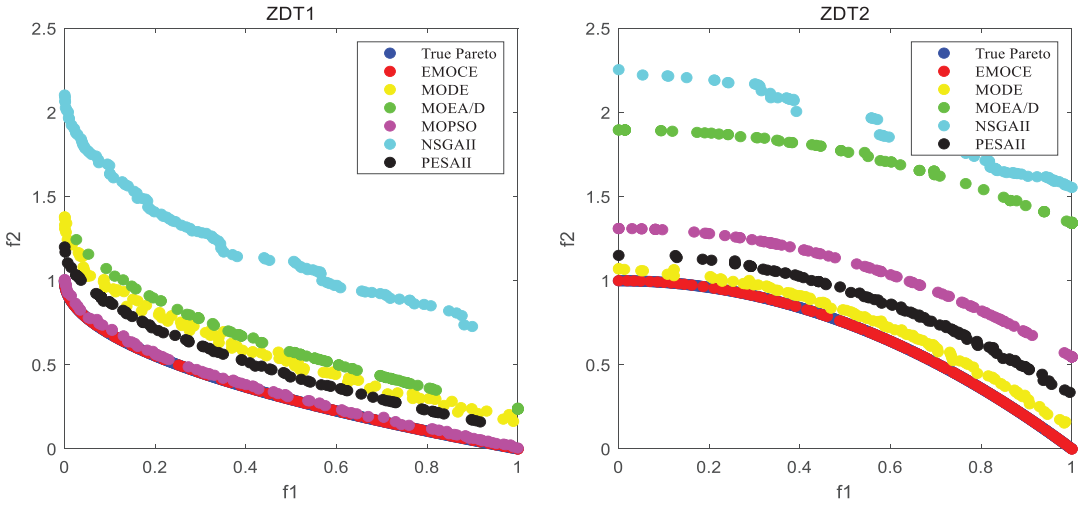

Figure 5: Comparison of algorithm pareto fronts on ZDT benchmark suite

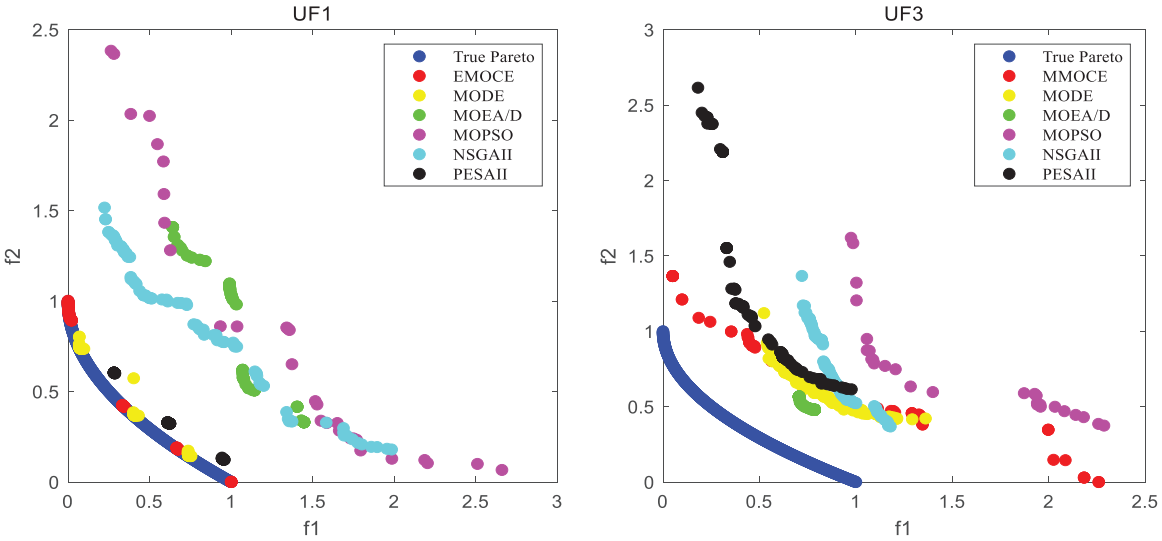

Figure 6: Comparison of algorithm pareto fronts on UF benchmark suite

3.2 Simulation Analysis of Robust Optimization Scheduling

In the microgrid case study examined herein, the system encompasses a photovoltaic unit and a wind turbine. A winter period characterized by pronounced uncertainty in solar and wind power generation is selected as the scheduling interval, thereby furnishing a rigorous testbed to substantiate the efficacy of the robust scheduling approach proposed in this paper. For computational expediency, the maximum deviation of actual power output from the day-ahead forecast for each renewable energy generation (REG) unit is stipulated at ±30%. The scheduling interval is delineated as 15 min. Moreover, the penalty coefficient for REG output uncertainty is calibrated to 10. Table 5 summarizes some key parameters used in the simulation.

Table 5: Key simulation data of the model

Key parameters	Value
Single-machine capacity (KW)	400
Initial SOC (equivalent to air pressure)/bar	55
SOC range (equivalent to air pressure)/bar	46~66

Fig. 7 depicts the day-ahead forecast profiles of power generation for the PV and wind stations, as well as the grid load trajectory.

In this study, the canonical multi-objective optimization algorithm, Multi-Objective Particle Swarm Optimization (MOPSO), is deployed as a comparative benchmark against the EMOCE algorithm. For Both algorithms use default parameters. Both algorithms are subjected to identical test cases, configured with a maximum iteration cap of 10,000, a population cohort of 100, and an external archive dimension of 60.

Under specified operational constraints where system spinning reserve requirements are satisfied with 55% probability threshold, Formulas (23)–(25) yield a robustness cost Γ_t = 0.632 and REG unit fluctuation coefficients $|\delta_{1,t}| = |\delta_{2,t}| = 0.316$, Fig. 8 presents the optimized Pareto-optimal fronts derived by both algorithms under these conditions, illustrating their solution space exploration capabilities. The results show that EMOCE achieves significantly lower operational costs and environmental dispatch expenditures compared to MOPSO. The proposed algorithm's Pareto front exhibits superior convergence and distribution characteristics, comprehensively outperforming MOPSO and establishing a clear Pareto-dominance relationship. This high-quality Pareto-optimal solution set enables strategic flexibility in decision-making: operators may prioritize extreme-region solutions for specialized objectives or select balanced compromise solutions through comprehensive performance metrics. The comparative analysis conclusively validates EMOCE's enhanced feasibility and superiority in multi-objective robust optimization frameworks.

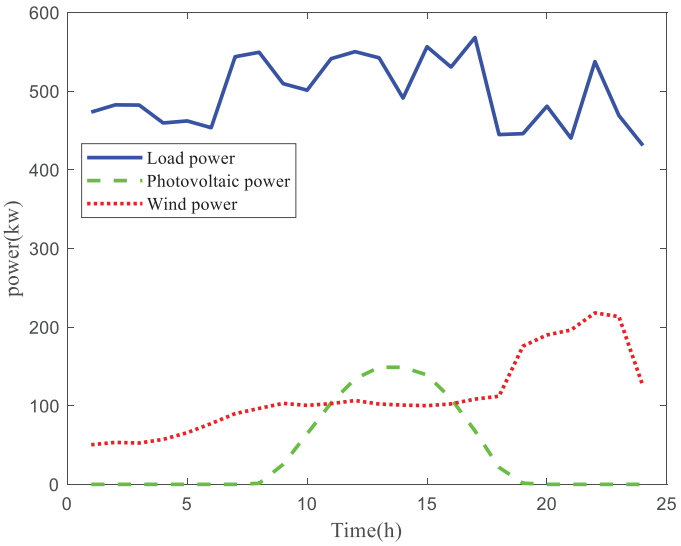

Figure 7: Load and prediction curves of PV, wind power

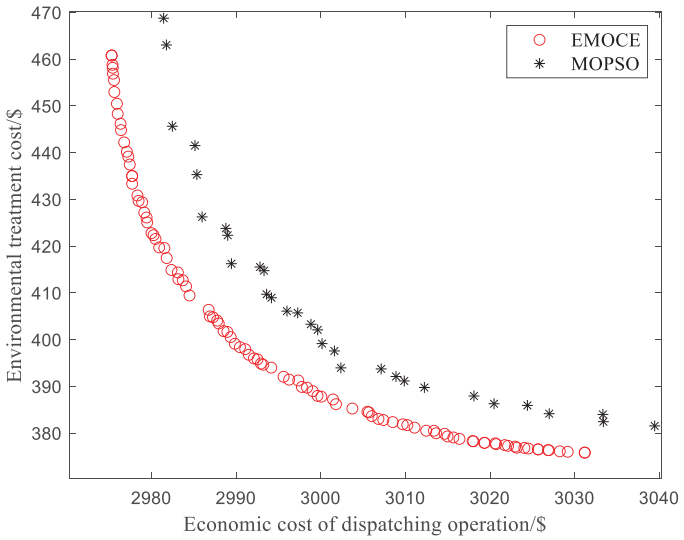

Figure 8: Multi-objective optimization results based on uncertainty budget decision

Utilizing the Fuzzy method, the compromise optimal solution of the EMOCE algorithm is identified, with the power output profiles of each unit depicted in Fig. 9. The results reveal that, due to the low upper limit of renewable energy output in this case, diesel generators and energy storage units primarily supply power throughout most periods. Before 6:00 a.m., insufficient wind and low solar irradiance necessitate high-power generation from diesel generators and energy storage to meet load demands. As solar irradiance and wind speeds increase, renewable energy output rises, allowing CAES to recharge. From 12:00 to 4:00 p.m., renewable energy maintains high output. In the evening, as solar power wanes, diesel generators resume primary output duties, complemented by increased wind power to support high nighttime loads. After midnight, energy storage ramps up output to fill power gaps.

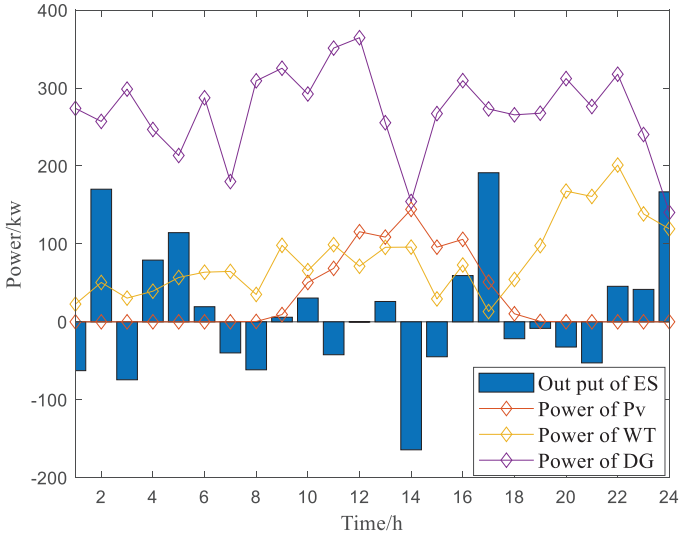

Figure 9: Output of each unit based on uncertainty budget decision

The resulting multi-objective optimization solution balances robustness and economic low-carbon performance, aligning with scheduling expectations.

3.3 Optimization Outcomes across Varied Uncertainty Budget Configurations

The test case adopted herein remains consistent with that employed in Section 3.2. To demonstrate the limitations of idealized traditional dispatch methods when handling renewable energy integration with stochastic fluctuations, Herein, the optimal compromise solution of the EMOCE set is extracted via the fuzzy method and aggregated into a single objective "Optimization Dispatch Cost F". The conventional single-objective particle swarm optimization (PSO) algorithm is employed for comparison, with results shown in Fig. 10.

Fig. 10 compares the dispatch cost curves of conventional approaches against our proposed robust optimization method under varying renewable output conditions. As illustrated, the boundary decision-based robust optimization exhibits significantly smaller cost variations compared to traditional dispatch as renewable energy volatility increases. This disparity arises because traditional optimization must frequently deviate from economically optimal generation schedules to maintain system reliability amid substantial PV/wind power fluctuations, consequently driving up operational costs. In contrast, the proposed robust optimization methodology inherently accommodates renewable generation uncertainties, thereby yielding more resilient dispatch solutions.

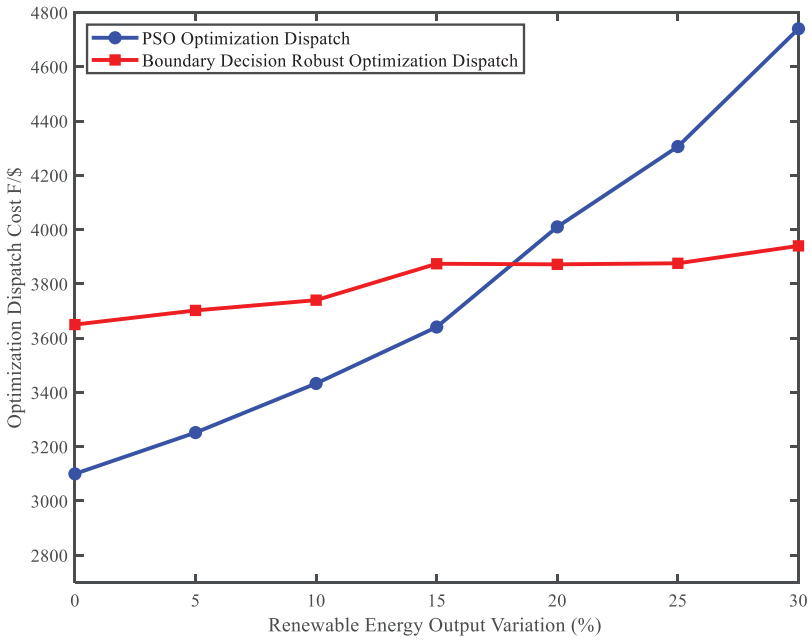

Figure 10: Relationship between comprehensive dispatch cost *F* and outputs variation of REG power plants

In real-world scheduling contexts, the tolerance for spinning reserve constraint violations is often modulated to align with operational demands, thereby dictating the choice of uncertainty budget. Here, the uncertainty budget Γ_t is calibrated to 0, 1, and 2. Focusing on photovoltaic and wind turbine units, the temporal power dispatch of REG units, optimized via the EMOCE algorithm, is illustrated in Fig. 11.

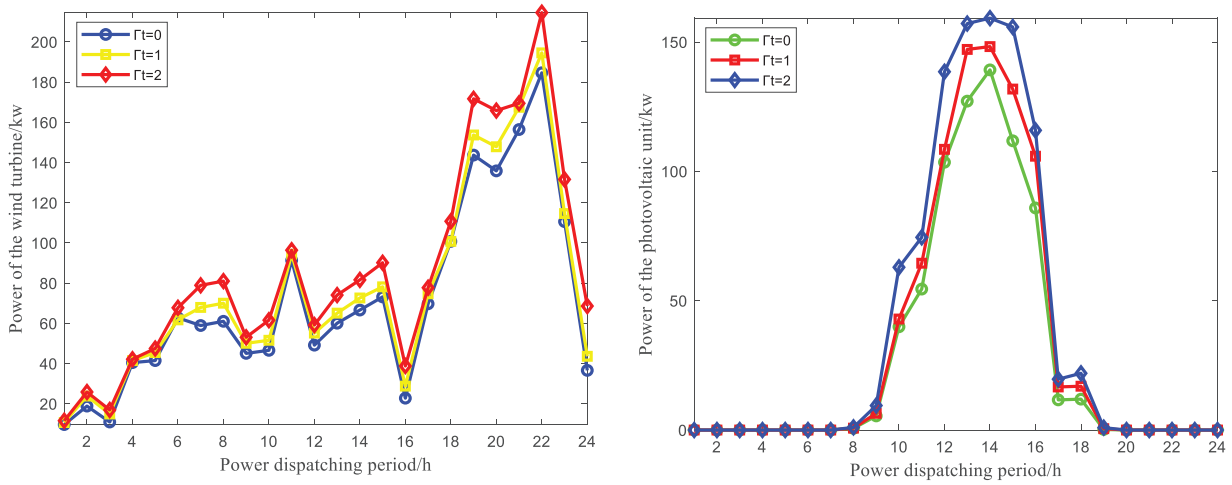

Figure 11: REG unit output at different uncertainty budgets

Corresponding to different uncertainty budgetvalues, the probabilities of spinning reserve constraint violations and the operational costs of the system are presented in Table 6.

Table 6: Comparative results of deterministic and robust scheduling under different uncertainty budgets

Scenario	Description	Constrained exceedance probability	Cost
Case 1	Deterministic scheduling scenario ($\Gamma_t = 0$)	80.6	2977
Case 2	Robust optimization scenario 1 ($\Gamma_t = 1$)	57.9	3096
Case 3	Robust optimization scenario 2 ($\Gamma_t = 2$)	35.2	3217
Case 4	Application of the deterministic theoretical solution within Robust Optimization Scenario 1 ($\Gamma_t = 1$)	/	3357
Case 5	Application of the deterministic theoretical solution within Robust Optimization Scenario 2 ($\Gamma_t = 2$)	/	3556

The importance of robust optimization is further demonstrated by the comparative experiments summarized in Table 6. As shown in the table, when the uncertainty budget Γ_t is set to 0, the dispatch output of renewable energy stations equals their forecasted values, indicating a deterministic model that ignores the stochastic nature of PV and wind power generation. While this deterministic approach yields the lowest theoretical dispatch cost compared to robust optimization scenarios that account for renewable energy fluctuations, implementing robust solutions within the deterministic framework reveals a different outcome. The resulting costs exceed those obtained through direct robust optimization because actual renewable generation often deviates from deterministic forecasts, necessitating costly real-time adjustments from conventional thermal and diesel generators to maintain system balance. This comparative analysis demonstrates that although robust optimization incurs additional theoretical costs compared to deterministic scheduling, it proves superior in practical applications by ensuring solution feasibility and achieving optimal actual economic performance when confronting real-world uncertainties.

Fig. 12 also demonstrates a corresponding increase in economic cost with the elevation of the Uncertainty Budget in the Pareto front, revealing a consistent pattern: achieving greater resilience against uncertainties invariably incurs higher operational costs. In practical power dispatch operations, when confronted with significant cost pressures, decision-makers may opt to moderately relax the probability requirements for constraint satisfaction. This strategy can partially mitigate scheduling costs but inevitably compromises system robustness. Therefore, to achieve a balanced trade-off between economic efficiency and robustness, the robustness cost parameter must be dynamically adjusted according to specific operational needs to identify the optimal equilibrium. This process highlights the complexity of decision-making in power system optimization and demonstrates the critical need for dynamically adaptive strategies to suit varying operational scenarios.

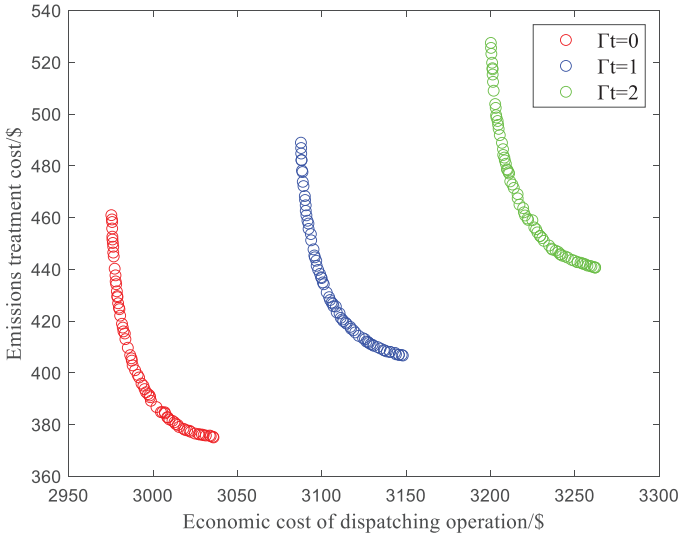

Figure 12: Pareto optimal frontier under different uncertainty budgets

4 Conclusions

To address the uncertainty of renewable energy generation in microgrid scheduling, this paper develops a framework based on robust optimization principles. By employing mathematical theories like Lagrangian transformation, the uncertainties in the model are eliminated, leading to a robust optimization strategy based on boundary decision-making under uncertainty. Moreover, the Cross-Entropy (CE) algorithm is enhanced by introducing crossover operators and parameter self-adaptive updates, resulting in an improved multi-objective CE algorithm for model solution. In the case study, the boundary decision-making method enables flexible selection of robustness cost according to actual needs, achieving a balance between the system's economic and environmental performance and its robustness. The results indicate the rationality and applicability of this decision-making approach. Meanwhile, the proposed multi-objective CE algorithm demonstrates superiority in solving environmental and economic scheduling problems. In conclusion, the integration of the proposed robust optimization strategy with the enhanced multi-objective CE algorithm yields a scheduling scheme with significant practical applicability and value.

Acknowledgement: Not applicable.

Funding Statement: This research was funded by Science and Technology Project of State Grid Zhejiang Electric Power Co., Ltd., grant number B311WZ23000C.

Author Contributions: Conceptualization, Junjian Wu and Zhenyu Zhou; methodology, Junjian Wu and Yejun Xiang; software, Jingliao Sun and Zhenyu Zhou; validation, Zhengchai Shi; formal analysis, Yejun Xiang and Zhenyu Zhou; investigation, Jingliao Sun; data curation, Zhengchai Shi; writing—original draft preparation, Junjian Wu and Jingliao Sun; writing—review and editing, Junjian Wu. All authors reviewed the results and approved the final version of the manuscript.

Availability of Data and Materials: Due to the nature of this research, participants of this study did not agree for their data to be shared publicly, so supporting data is not available.

Ethics Approval: Not applicable.

Conflicts of Interest: The authors declare no conflicts of interest to report regarding the present study.

Abbreviations

MG	Microgrid
REG	Renewable Energy Generation
SO	Stochastic Optimization
CCP	Chance Constrained Programming
RO	Robust Optimization
SO	Stochastic Optimization
CE	Cross-Entropy Algorithm
NSGA-II	Nondominated Sorting Genetic Algorithm II
EMOCE	External Files-Based Multi-Objective Cross-Entropy Algorithm
PV	Photovoltaic
WT	Wind Turbine
CAES	Compressed-Air Energy Storage
MOPSO	Multi-Objective Particle Swarm Optimization

References

1. Ahmad S, Shafiullah M, Ahmed CB, Alowaifeer M. A review of microgrid energy management and control strategies. IEEE Access. 2023;11(1):21729–57. doi:10.1109/ACCESS.2023.3248511.
2. Cui Y, Xu Y, Wang Y, Li Y, Zhao Y. Multi-microgrid optimization operation strategy considering nonlinear conditions and renewable energy uncertainty: a data-driven method. IEEE Trans Ind Appl. 2024;61(1):1533–45. doi:10.1109/TIA.2024.3371966.
3. Divya S, Paramathma MK, Sheela A, Kumar SD. Hybrid renewable energy source optimization using black widow optimization techniques with uncertainty constraints. Meas Sens. 2024;31:100968. doi:10.1016/j.measen.2023.100968.
4. Zhao T, Pan X, Yao S, Ju C, Li L. Strategic bidding of hybrid AC/DC microgrid embedded energy hubs: a two-stage chance constrained stochastic programming approach. IEEE Trans Sustain Energy. 2018;11(1):116–25. doi:10.1109/TSTE.2018.2884997.
5. Song Y, Xia M, Yang L, Chen Q, Su S. Multi-granularity source-load-storage cooperative dispatch based on combined robust optimization and stochastic optimization for a highway service area micro-energy grid. Renew Energy. 2023;205:747–62. doi:10.1016/j.renene.2023.02.006.
6. Zanvettor GG, Casini M, Giannitrapani A, Paoletti S, Vicino A. A chance-constrained programming approach to optimal management of car-rental fleets of electric vehicles. Sustain Energy Grids Netw. 2025;41(1):101587. doi:10.1016/j.segan.2024.101587.
7. Hemmati M, Bayati N, Ebel T. Integrated optimal energy management of multi-microgrid network considering energy performance index: global chance-constrained programming framework. Energies. 2024;17(17):4367. doi:10.3390/en17174367.

8. Wu S, Qi X, Li X, Liu X, Tong B, Zhang F, et al. Collaborative robust dispatch of electricity and carbon under carbon allowance trading market. Glob Energy Interconnect. 2024;7(4):391–401. doi:10.1016/j.gloei.2024.08.003.
9. Gilani H, Sahebi H, Pishvaee MS. A data-driven robust optimization model for integrated network design solar photovoltaic to micro grid. Sustain Energy Grids Netw. 2022;31(1):100714. doi:10.1016/j.segan.2022.100714.
10. Okido S, Takeda A. Economic and environmental analysis of photovoltaic energy systems via robust optimization. Energy Syst. 2013;4(3):239–66. doi:10.1007/s12667-013-0077-1.
11. Akbari K, Nasiri MM, Jolai F, Ghaderi SF. Optimal investment and unit sizing of distributed energy systems under uncertainty: a robust optimization approach. Energy Build. 2014;85:275–86. doi:10.1016/j.enbuild.2014.09.009.
12. Aguilar D, Quinones JJ, Pineda LR, Ostanek J, Castillo L. Optimal scheduling of renewable energy microgrids: a robust multi-objective approach with machine learning-based probabilistic forecasting. Appl Energy. 2024;369:123548. doi:10.1016/j.apenergy.2024.123548.
13. Tinajero GDA, Vasquez JC, Guerrero JM, editors. Flexible power flow for controlled islanded microgrids including battery energy storage systems. In: Proceedings of the IECON 2023—49th Annual Conference of the IEEE Industrial Electronics Society; 2023 Oct 16–19; Singapore. doi:10.1109/IECON51785.2023.10312071.
14. Kudva A, Sorourifar F, Paulson JA. Constrained robust Bayesian optimization of expensive noisy black-box functions with guaranteed regret bounds. AIChE J. 2022;68(12):e17857. doi:10.1002/aic.17857.
15. Mak S, Jeff Wu C. Analysis-of-marginal-tail-means (ATM): a robust method for discrete black-box optimization. Technometrics. 2019;61(4):545–59. doi:10.1080/00401706.2019.1593246.
16. Wang D, Zhang C, Li J, Zhu L, Zhou B, Zhou Q, et al. A novel interval power flow method based on hybrid box-ellipsoid uncertain sets. IEEE Trans Power Syst. 2024;39(4):6111–4. doi:10.1109/TPWRS.2024.3391921.
17. Luo G-M. Research on robust cooperative dual equilibrium with ellipsoidal asymmetric strategy uncertainty. Chin Q J Math. 2019;34(4):431. (In Chinese). doi:10.13371/j.cnki.chin.q.j.m.2019.04.008.
18. Bertsimas D, Sim M. The price of robustness. Oper Res. 2004;52(1):35–53. doi:10.1287/opre.1030.0065.
19. Gao C, Feng Y, Tong X, Jin Y, Liu S, Wu P, et al. Modeling urban encroachment on ecological land using cellular automata and cross-entropy optimization rules. Sci Total Environ. 2020;744:140996. doi:10.1016/j.scitotenv.2020.140996.
20. Kalantari F, Hosseininezhad SJ. A Multi-objective Cross Entropy-based algorithm for sustainable global food supply chain with risk considerations: a case study. Comput Ind Eng. 2022;164:107766. doi:10.1016/j.cie.2021.107766.
21. Gong Z, Jiang Y, Dai J. Node importance ranking algorithm based on cross entropy. J Univ Electron Sci Technol China. 2023;52(6):944–53. doi:10.12178/1001-0548.2023058.
22. Yan Y, Zhang C, Li K, Tian C, Wang F. An active control strategy for composited energy storage with compressed air energy storage in micro-grid. Trans China Electrotech Soc. 2017;32(20):231–40. (In Chinese). https://doi.org/10.19595/j.cnki.1000-6753.tces.160628.
23. Park H, Baldick R. Integration of compressed air energy storage systems co-located with wind resources in the ERCOT transmission system. Int J Electr Power Energy Syst. 2017;90:181–9. https://doi.org/10.1016/j.ijepes.2017.01.021.
24. Popp J, Deutscher J. Optimizing the efficiency of a single-cylinder diesel generator by using optimal and extremum seeking control. Forsch Im Ingenieurwesen. 2017;81:421–35. https://doi.org/10.1007/s10010-017-0251-z.
25. Peng C, Xie P, Chen C. Adjustable robust optimal dispatch of power system with large-scale photovoltaic power stations. Proc CSEE. 2014;34(25):4324–32. https://doi.org/10.13334/j.0258-8013.pcsee.2014.25.015.
26. An S, Wang W, Yang S. Vector design optimizations using an improved cross-entropy method. IEEE Trans Magn. 2015;51(3):1–4. doi:10.1109/TMAG.2014.2357219.